Large-scale density-functional calculations on silicon divacancies

Jun-ichi Iwata,[1,2] Kenji Shiraishi,[2,3] and Atsushi Oshiyama[1,2,3]
[1]*Center for Computational Sciences, University of Tsukuba, Tennodai, Tsukuba 305-8577, Japan*
[2]*CREST, Japan Science and Technology Agency, 4-1-8 Honcho, Kawaguchi, Saitama 332-0012, Japan*
[3]*Graduate School of Pure and Applied Sciences, University of Tsukuba, Tennodai, Tsukuba 305-8571, Japan*
(Received 23 May 2007; published 24 March 2008)

We have performed total-energy electronic-structure calculations in the density-functional theory for the divacancy in Si using our real-space finite-difference pseudopotential method. Supercell models containing up to 1000 sites as well as a cluster model containing 432 atoms are used to simulate the divacancy in an otherwise perfect crystal. We have found that the resonant bond configuration is the most stable structure, the small pairing configuration is the next, and the large pairing configuration is the least stable for negatively and positively charged as well as neutral divacancies in the supercell model. The energy differences among the three configurations are found to be the order of 10 meV. Considering situations of ESR measurements, we have also performed the total-energy electronic-structure calculations under uniaxial stress along the ⟨110⟩ direction. We have found that induced strains alter the energetics and the pairing configurations become most stable with increasing strains. We argue that the ground state configuration of the Si divacancy is the resonant bond configuration and the pairing configurations become stable under the uniaxial stress and are detected by the EPR measurements.

DOI: 10.1103/PhysRevB.77.115208 PACS number(s): 61.72.J−, 61.72.Bb, 71.55.Cn, 71.15.Mb

I. INTRODUCTION

Defects in materials affect properties of the host materials substantially. In covalent semiconductors, for instance, vacancies generate dangling bonds around and thereby induce deep electron states in the energy gap. Those deep levels decisively modify transport and optical properties of the semiconductors, even if the vacancy is a ppm host atoms.

An interesting feature in vacancies in semiconductors is caused by multiplicity of charge states: When the Fermi level varies in the energy gap, the deep levels accommodate different numbers of electrons and thus the vacancy becomes several different charge states depending on the Fermi-level position. The deep level is occasionally degenerate owing to high-symmetry atomic configurations around the vacancy. Partial occupation with electrons of the degenerate deep level may induce symmetry-lowering distortion around the vacancy due to the Jahn–Teller effect.[1,2] Multiplicity of charge states therefore leads to a variety of atomic structures and of resulting electronic properties.

Microscopic structures around the vacancy have been indeed studied extensively for silicon.[3] Electron spin resonance (ESR) measurements[4–6] along with density-functional calculations[7–11] have clarified that the monovacancy V_1 in Si exhibits pairing-type Jahn–Teller distortion in which each two of the four neighboring Si atoms are rebonded, being associated with medium- or long-range lattice relaxation of surrounding atoms. The change in the Fermi-level position in the energy gap results in the existence of four different charge states, V_1^{+2}, V_1^{+1}, V_1^{0}, and V_1^{-1}, each of which is associated with or without a particular paring distortion. The Jahn–Teller energy, i.e., the energy gain due to the Jahn–Teller distortion, is typically a few tenths of eV.

The divacancy V_2 which is also an abundant point defect in Si has been also studied for many years. Yet, to our surprise, there is no consensus about atom-scale structures of the divacancy.

Removing two neighboring Si atoms in the diamond structure generates an ideal (unrelaxed) divacancy V_2 where atomic arrangements are of D_{3d} point-group symmetry (Fig. 1). The electron states induced by the ideal divacancy are classified into four states in terms of irreducible representations of D_{3d}:[12,13] a_{1g} and a_{1u} states resonating in valence bands and doubly degenerate e_u and e_g states in the energy gap. For the neutral divacancy, six electrons from the neighboring six dangling bonds occupy the a_{1g} and a_{1u} completely, and then e_u partially. In a case that the pairing distortion takes place as in the monovacancy due to the Jahn–Teller effect, the e_u splits into a lower b_u and an upper a_u states, whereas the e_g splits into a lower a_g and an upper b_g states, as schematically shown in Fig. 2(a).

However, this naive paring relaxation is inconsistent with the ESR measurements.[12,14–16] The ESR measurements have detected the positively charged (V_2^+) and the negatively charged (V_2^-) divacancies in *p*-type and *n*-type Si, respectively. The symmetry of the atomic structures of V_2^+ and V_2^- has been determined to be C_{2h}. Moreover, it is shown that the wave functions of the electron states detected by the ESR

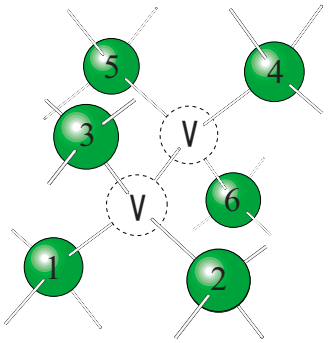

FIG. 1. (Color online) Schematic view of divacancy. Vacancies are depicted by dashed circles.

 ©2008 The American Physical Society

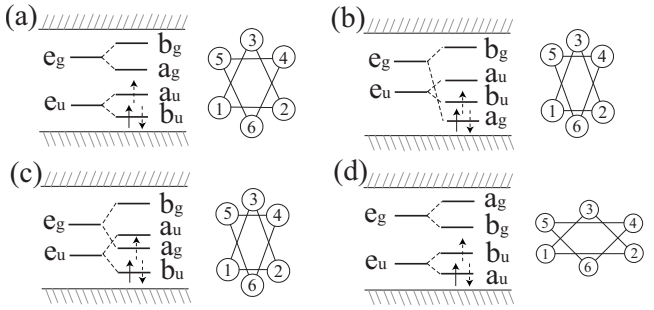

FIG. 2. Schematic views of electron states induced by the divacancy along with corresponding relaxation patterns of surrounding six atoms. (a) In the pairing distortion, e_u splits into a lower b_u and an upper a_u, whereas e_g splits into a lower a_g and an upper b_g. [(b) and (c)] The large pairing may cause exceptionally large splittings. (d) The level splitting in the resonant-bond relaxation. In positively charged V_2, an electron depicted by a solid arrow occupies the corresponding state, whereas in negatively charged V_2 additional electrons depicted by dashed arrows occupy the states. a_g^2 and b_u^2 cited in text are depicted as a_g and b_u here for simplicity.

measurements have amplitudes on a mirror plane in C_{2h} symmetry both for V_2^+ and V_2^-. The mirror plane is the (110) plane on which the nearest-neighbor atoms labeled with 3 and 6 in Fig. 1 are located. The wave functions b_u and a_g do have amplitudes on the mirror plane, whereas a_u and b_g have node on the plane. The simple pairing picture depicted in Fig. 2(a) is thus incapable to explain the ESR data for V_2^-.

Watkins and Corbett[12] have therefore proposed a large-pairing (LP) model shown in Fig. 2(b) where paring distortion is exceptionally large so that a_g and b_u are the states which are detected by ESR for the positive and the negative V_2, respectively. This model nicely explains the ESR measurements, except for an unclear reasoning for such large Jahn–Teller splitting due to the pairing.

It is of note that the LP distortion may induce the electronic structure shown in Fig. 2(c) which is also consistent with the ESR measurements.

An alternative has emerged from a theoretical side. Saito and Oshiyama proposed a new relaxation pattern around the divacancy called the resonant bond (RB) configuration.[17] Based on the local density approximation (LDA) in the density-functional theory (DFT), they have found that the pairing of two atoms among three neighboring Si [either the atoms (123) or the atoms (456)] is absent in the RB configuration and resonant bonds among the three neighbors comes up instead. Inward lattice relaxation is also accompanied. In the RB configuration, directions of displacements of neighboring atoms are reverse to the directions in the pairing configurations so that the ordering of the electronic levels also become reverse, as in Fig. 2(d). Saito and Oshiyama have proposed that the negatively charged V_2 is the RB type with the ESR-detected state being the b_u, whereas the positively charged V_2 is the pairing type with again the b_u being detected by ESR on the basis of their total-energy calculations using periodic supercell models with the plane-wave basis set.[17] Subsequent calculations using similar techniques in DFT supports the RB configuration as a ground state in Si (Refs. 18, 19, and 21) and also in compound semiconductors.[20] The supercell used in these calculations contain relatively small number of atoms ranging from 64 to 216 atomic sites.

A support for the LP configuration depicted in Fig. 2(c) has come from another calculation based on the LDA in DFT. Ögüt and Chelikowsky[22,23] has performed LDA calculations for Si clusters in which boundary Si atoms are terminated by hydrogen atoms. They have systematically increased the size of the cluster, up to the isotropic $Si_{316}H_{198}$ and the ⟨110⟩-elongated $Si_{246}H_{186}$, and found that the LP configuration, as in Fig. 2(c), is energetically most favorable for V_2^+, V_2^0, and V_2^-. They have also found that the LP configuration is not realized in small-size clusters. The calculational scheme adopted by Ögüt and Chelikowsky is different from the plane-wave supercell-model calculations mentioned above: i.e., the real-space finite-difference method in which kinetic operators are treated by finite difference formula and all the quantities are computed on grid points in real space.

Apparent discrepancy among several LDA calculations described above is related to insufficiency of theoretical methodology in treating point defects in an otherwise perfect crystal. In the supercell model, point defects are arranged periodically so that all the electron states including deep states in the energy gap are delocalized in principle as Bloch states. In the cluster model, all the electron states decay outside the cluster so that continuum states in the energy bands are not described in principle. It is unclear how the difference in boundary conditions of electron states affects the energetics of point defects.[24] Further, the size of either the supercell or the cluster which mimic the point defect in an otherwise perfect crystal certainly causes ambiguity in the lattice relaxation and thereby in the energetics.

A practical approach to get rid of the above discrepancy is to perform both supercell-model calculations and cluster-model calculations with sufficient number of atoms on equal footing, and then examine the difference and the agreement about the relaxation of surrounding atoms and the resulting energetics. This is the purpose of the present work. We developed a real-space finite-difference DFT code and performed the total-energy electronic-structure calculations for both supercell models and cluster models containing V_2 in Si. In the present supercell calculations, the number of atomic sites ranges from 64 to 1000, whereas the cluster calculations treat several sizes including the largest cluster treated in the past. We have found that the RB configuration is energetically favorable for V_2^- in the supercell model, whereas the small-pairing (SP) configuration is favorable in the cluster model. The LP configuration is found to be unfavorable both in the supercell and cluster calculations.

Considering that uniaxial stress is applied in EPR measurements to determine the atomic structure, we have further performed the total-energy calculations for the negatively charged V_2 under uniaxial stress. We have found that the pairing configurations, SP and LP configurations, become energetically favorable under the stress condition. This finding reasonably explains the discrepancy between the LDA calculations and the ESR measurements in the past as to the defect structure.

In Sec. II, we explain a chemical picture of deep states induced by the divacancy in terms of nearest dangling-bond

orbitals. This provides intuition about the level ordering of the deep states. Our real-space calculation scheme is described in Sec. III. Section IV provides calculated results for energetics, atomic structures, and electron states of the divacancy in Si. Section V summarizes findings in the present work.

II. MOLECULAR ORBITAL PICTURE OF DEEP LEVELS

Deep electron states are generally localized around vacancies. It is therefore useful to consider wave functions of the deep states in terms of linear combinations of nearest dangling-bond orbitals. The obtained molecular orbital picture assists in examining the order of the deep energy levels.

Let us consider six dangling-bond orbitals, $\psi_1 \sim \psi_6$, at the nearest six atoms around the two vacant sites (Fig. 1). Those dangling-bond orbitals are arranged to be six basis functions ψ_ν of irreducible representations of C_{2h} point group of V_2. The explicit representation of the basis functions are as follows:

$$\psi_{a_g} = \begin{cases} \psi_1 + \psi_2 + \psi_4 + \psi_5 \\ 2\psi_3 + 2\psi_6, \end{cases}$$

$$\psi_{b_g} = \psi_1 - \psi_2 + \psi_4 - \psi_5,$$

$$\psi_{a_u} = \psi_1 - \psi_2 - \psi_4 + \psi_5,$$

$$\psi_{b_u} = \begin{cases} \psi_1 + \psi_2 - \psi_4 - \psi_5 \\ 2\psi_3 - 2\psi_6. \end{cases}$$

For the representations a_g and b_u, there are two possible linear combinations. Hence, we reach the following basis for those four representations;

$$\psi_{a_g^1} = \psi_1 + \psi_2 + \psi_4 + \psi_5 + \lambda(2\psi_3 + 2\psi_6),$$

$$\psi_{a_g^2} = 2\psi_3 + 2\psi_6 - \lambda(\psi_1 + \psi_2 + \psi_4 + \psi_5),$$

$$\psi_{b_u^1} = \psi_1 + \psi_2 - \psi_4 - \psi_5 + \mu(2\psi_3 - 2\psi_6),$$

$$\psi_{b_u^2} = 2\psi_3 - 2\psi_6 - \mu(\psi_1 + \psi_2 - \psi_4 - \psi_5),$$

with positive constants λ and μ.

The corresponding energy level ε_ν of each state is related to the number and locations of nodes of the basis ψ_ν, and the order of the energy levels is qualitatively predictable in some cases. The criteria are the following: (1) increasing the number of nodes of the orbital raise the energy, and (2) nodes on the plane where atoms (1,2,3) or atoms (4,5,6) in Fig. 1 are located costs more in energy than nodes between the planes. Among the six basis functions above, only the a_g^1 and the b_u^1 basis functions have a node neither on the (1,2,3) nor on the (4,5,6) plane. The corresponding energy levels are therefore expected to be lower than other four levels. Since a_g^1 and b_u^1 are the bonding and the antibonding characters, respectively, between the (1,2,3) and the (4,5,6) planes, we reasonably conclude that

$$\varepsilon_{a_g^1} < \varepsilon_{b_u^1} < \text{other energy levels}.$$

The characters of these a_g^1 and b_u^1 are the same with those of a_{1g} and a_{1u} of D_{3d} symmetry which are resonant in valence bands in the ideal V_2.

The remaining four states, a_u, b_g, a_g^2, and b_u^2, which split from corresponding gerade and ungerade e representations in D_{3d} symmetry, are expected to appear in the energy gap. When we consider ψ_{a_u} and ψ_{b_g}, they have nodes between atoms 1 and 2 on the (1,2,3) plane and between atoms 4 and 5 on the (4,5,6) plane. Further, the ψ_{b_g} has a node between the planes. Hence, it is likely that

$$\varepsilon_{a_u} < \varepsilon_{b_g}. \tag{1}$$

The node in the planes for $\psi_{a_g^2}$ and $\psi_{b_u^2}$ are of the same type: Both have nodes between the atom pair (1,2) and atom 3 on the (1,2,3) plane and between the atom pair (4,5) and atom 6 on the (4,5,6) plane. Further, the $\psi_{a_g^2}$ has an additional node between the (1,2,3) and (4,5,6) planes. We therefore expect that

$$\varepsilon_{b_u^2} < \varepsilon_{a_g^2}. \tag{2}$$

Further discussion as to the order of the energy levels depend on the detailed structures of the reconstructed divacancy. In the pairing configuration where atoms (1,2) and (4,5) are paired, the node between those atoms is energetically unfavorable. When we consider the gerade representations, $\psi_{a_g^2}$ and ψ_{b_g}, the latter has a node between the atom pair, whereas the former does not. Then,

$$\varepsilon_{a_g^2} < \varepsilon_{b_g}. \tag{3}$$

Similarly, between the two ungerade states,

$$\varepsilon_{b_u^2} < \varepsilon_{a_u}. \tag{4}$$

As to the order between ε_{a_u} and $\varepsilon_{a_g^2}$, the corresponding two basis functions have different patterns of nodes to each other. Hence, the order depends on the amount of the pairing. When the paring becomes enhanced, the a_g^2 state is likely to be lower. From the discussion above, it is reasonable to conclude that the level structure in the pairing distortion is shown in either Fig. 2(a) or 2(c). From the discussion leading to Eq. (2), the level structure shown in Fig. 2(b) is unlikely.

In the RB configuration, the directions of the displacements of atoms (1,2) and (4,5) are reverse to the corresponding directions in the pairing distortion. Then, Eqs. (3) and (4) becomes reverse: i.e.,

$$\varepsilon_{b_g} < \varepsilon_{a_g^2}, \tag{5}$$

$$\varepsilon_{a_u} < \varepsilon_{b_u^2}, \tag{6}$$

in the RB configuration. The order of $\varepsilon_{b_u^2}$ and ε_{b_g} depends on the detailed atomic structure and it is difficult to predict from simple molecular-orbital pictures. Then, we reasonably conclude that the level structure in the RB configuration is shown in Fig. 2(d), where b_u and b_g may be reverse depending on the detailed structure.

III. REAL-SPACE DENSITY-FUNCTIONAL CALCULATIONS

Total-energy electronic-structure calculations performed in the present work are based on the density-functional theory[25,26] with the LDA[27] and the generalized gradient approximation[28] (GGA) using norm-conserving pseudopotentials.[29,30] A standard way to solve the Kohn–Sham equation, which is a variational equation of the total energy with respect to the electron density, is to introduce a basis set to represent effective one-electron states (Kohn–Sham states) and thus the electron density. In the real-space formulation,[31] grids in real space are introduced instead of basis sets and wave functions, electron density and potentials are computed at each grid point. Accuracy of the computation is guaranteed by systematically decreasing the separation between grid points. This corresponds to the systematic increase of the number of plane waves in the plane-wave basis-set approach and thereby provides practically accurate solutions of Kohn–Sham equations. We have developed an efficient real-space code,[32] which we use in the present work. The results obtained by our real-space code agree perfectly with those obtained by our plane-wave basis-set code.[33]

In our real-space formulation, the kinetic energy operator is represented by the high-order finite-difference operator using values of corresponding functions at nearby grid points. The order of the finite-difference formula suitable for practical computations is linked to a choice of the spacing of grid points. We have examined a variety of possibilities and obtained an optimum set of parameters in which the sixth order formula using values at 12 nearby grid points in one direction for the Laplacian operation is adopted with five to six grid points between adjacent two atomic sites.

One of the advantages in the real-space formulation is its being almost free from a spell of fast Fourier transform (FFT). In the standard basis-set approach such as the plane-wave basis-set approach, FFT is indispensable in handling convolutions in Hamiltonian operations. Yet, FFT becomes a serious burden when we attempt to implement codes on the parallel architecture due to communications among all processors. In the real-space formulation, it is unnecessary to use FFT in Hamiltonian operations. In calculations of long-range Hartree potentials, it may be useful to use FFT. Even for the calculations of Hartree potentials, solving Poisson equations in real space may be an alternative in massively parallel computations. In the present version of our code, we use FFT only in calculating Hartree potentials.

In our parallel code, we divide the target system into blocks, depending on the available resources. Each processor is responsible for each block. Values of required functions in each block are stored in each local memory. Most computations are performed locally on each processor. Communications among different processors occur only when the computations of finite-difference operations and inner products are performed. In the case that we use FFT to compute Hartree potentials, it is convenient to store electron density at all memories and perform FFT at all processors. The computational cost for FFT for the present size of targets is of small portion.

Kohn–Sham equations are solved iteratively by either conjugate-gradient minimization[10,34] or residual minimization technique.[35] The latter technique substantially accelerates our computations since the Gram–Schmidt orthogonalization is unnecessary in minimization iterations. Atomic geometries are also optimized by the conjugate-gradient minimization technique using calculated Helmann–Feynman forces.

To simulate nuclei and core electrons, norm-conserving pseudopotentials of Troulier–Martins type[30] are used with the Kleinman–Bylander approximation.[36] Nonlocality of pseudopotentials are treated in real space, which has an advantage in computational scaling with respect to the system size N (number of atoms): i.e., $O(N^2)$ rather than $O(N^3)$ scaling is possible in real-space treatment. In this case, filtering the high-energy components of the pseudopotentials is important to reduce the numerical errors. We adopt the mask-function method[37] in the filtering.

The exchange-correlation potential is given by the functional derivative of the exchange-correlation energy with respect to the electron density, and thus, in GGA, contains the first and the second derivatives of the energy with respect to the density gradient and to the density itself. Using analytical expressions for those derivatives in the real-space treatment may cause numerical inconsistency between the exchange-correlation energy and potential. To avoid the problem, we express the exchange-correlation energy as an integral over real-space grids and obtain the potential as its partial derivative with respect to the density at each grid point, following the procedure proposed by Balbás *et al.*[38] in our GGA calculations.

Another advantage in the real-space formulation is the flexibility to treat boundary conditions of wavefunctions. In the plane-wave basis-set approach, supercell models where all the electron wavefunctions satisfy periodic boundary conditions are imperative. The real-space approach is capable of treating cluster models as well as supercell models in principle. In the present real-space calculations, both supercell models and cluster models are treated on equal footing, thereby elucidating reasons for the discrepancy in the past regarding the defect structure of V_2 in Si.

In the present calculations for the divacancy in crystalline Si, we generate norm-conserving pseudopotentials for Si and H with core radii of 1.3 and 0.66 Å, respectively. We include s and d components of the nonlocal projectors with p local potential for Si and include only local s potential for H. Corresponding to the core radii, we adopt equal-space grids with the separation of $h=0.38$ Å. We have obtained the convergence of total-energy difference within 10 meV with this spacing. The spacing corresponds to the cutoff energy $E_c=18$ Ry in the plane-wave basis-set scheme when we use the relation $E_c=(\pi/h)^2$. This scheme provides the lattice constant of 5.38 Å in LDA and 5.48 Å in GGA, which are 0.9% shorter and 1% longer than the experimental value, respectively. In the present calculations, we use these values for the lattice constants. The structure optimization has been performed until the remaining forces in the optimized geometries are less than 4 mRy/Å.

We use both supercell models and cluster models. In the supercell model, we adopt a series of cubic unit cells in which 64, 216, 512, or 1000 atomic sites, respectively, are included, and all the atomic positions are relaxed using cal-

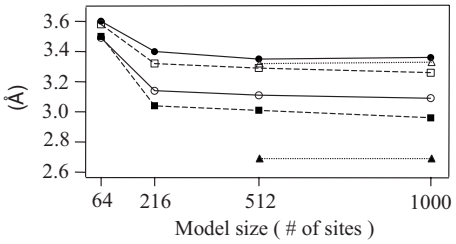

FIG. 3. Rebond lengths of nearest neighbor Si atoms, d_{12} (black markers) and d_{23} (open markers), as a function of supercell size in RB configuration (solid lines with circles), SP configuration (broken lines with squares), and LP configuration (dotted lines with triangles).

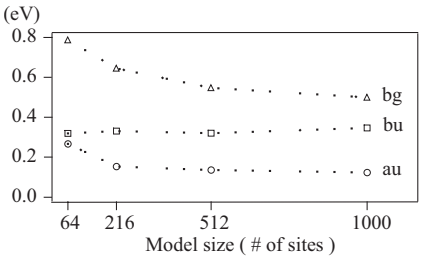

FIG. 4. Deep level positions of V_2^- in RB configuration as a function of supercell size. The lower three deep level positions, a_u, b_u, and b_g, measured from the top of the valence bands are shown.

culated forces. Brillouin-zone integral is done using Γ point sampling. In the cluster model, we adopt a $Si_{246}H_{186}$ cluster in which Si atoms within the 13th shell around V_2 and additional Si atoms up to the 25th shell along the direction $[1\bar{1}0]$ are included. The direction is the rebond direction in the pairing configuration. Hydrogen atoms are attached to the boundary Si atoms. Both the H and boundary Si atoms are fixed in the structure optimization processes. The remaining 138 Si atoms inside unconnected with H atoms are relaxed by using the calculated forces, as is described above, and the remaining forces in the optimized geometries are less than 4 mRy/Å. This cluster is identical to the largest cluster adopted in the previous real-space cluster calculations for V_2 in Si.[22,23] We take a vacuum region around the cluster where the calculated wave functions decay. We have found that the vacuum region with a dimension of 6–10 Å surrounding the cluster is sufficient to obtain converged results. It is of note that the unit cell of 1000 sites in the supercell model contains all the Si atoms which are treated in the previous cluster calculations.

IV. RESULTS AND DISCUSSION

In this section, we present calculated energetics, atomic structures, and electron states obtained in the supercell model and in the cluster model. Most of the results presented here are obtained by the LDA calculations unless stated otherwise.

In the supercell approach, we take a cubic unit cell and increase its size from 64 sites to 1000 sites. We have explored the sufficient supercell size by examining variation of the atomic structure of V_2^- with increasing the supercell size. The distance between nearest neighbor Si atoms 1 and 2 d_{12} and the distance between 2 and 3 d_{23} are the principal structural parameters. Figure 3 shows the calculated d_{12} and d_{23} for the RB, LP, and SP configurations of V_2^-. We observe that sufficient convergence is achieved with the 1000-site supercell: For instance, the differences in the calculated d_{12} and d_{23} between the 512-site cell and the 1000-site cell calculations are 0.01 and 0.02 Å, respectively, in the RB configuration. These differences are already close to the limitation of accuracy in LDA.

We have also examined overall structural differences between 512-site-cell and 1000-site-cell calculations. The root mean square of the coordinate difference of 510 atoms in the 512-site cell and 1000-site cell is 0.01 Å. Further, in the 1000-site-cell calculations, the root mean square of displacements from corresponding unrelaxed sites of outer 488 atoms which are not included in the 512-site cell is found to be 0.01 Å. The maximum difference in the coordinate for each atom between the 512-site-cell and the 1000-site-cell calculations is 0.05 Å. These values are also close to the LDA limitations. We thus conclude that the obtained atomic geometry around V_2 sufficiently converges with the present size of supercells.

The convergence of electronic level structures are also examined. Figure 4 shows level positions of the lower three deep levels in the RB configuration of V_2^- as a function of the supercell size. The differences in the level positions between the 512-site-cell and 1000-site-cell calculations are 13–35 meV, which is much smaller than expected ambiguities in the LDA calculations. In the cluster models, the separations of these energy levels are the same as those in the supercell model within 0.1–0.2 eV, in spite of the large difference in the band gap (0.5 and 1.7 eV in the supercell and the cluster models, respectively). This means that the magnitude of the Jahn–Teller distortions which are determined by those level separations and stiffness of the lattice can be described properly both in supercell and in cluster models.

The formation energy E_f^Q of the divacancy V_2^Q with charge Q is defined as

$$E_f^Q = E_{V_2^Q} - E_0 + 2\mu_{\mathrm{Si}} + \mu_e Q, \tag{7}$$

where $E_{V_2}^Q$ and E_0 are the total energies of the divacancy and the perfect crystal, and μ_{Si} and μ_e are the chemical potential of Si atom and the electron. It is plausible to use the total energy per atom in Si crystal for μ_{Si}, and μ_e is an external parameter peculiar to each sample. We have calculated the formation energies of negatively charged (V_2^-) divacancy with the RB, LP, and SP configurations using a standard procedure in supercell models.[39] When μ_e is at the middle of the energy gap, E_f^- is 5.9 eV in the present 1000-site-cell calculations. (Differences in E_f^- among the RB, LP, and SP configurations are less than 0.1 eV and will be discussed below.)

Table I summarizes the calculated results for energetics and bond lengths for negatively charged, neutral, and positively charged V_2 using our supercell models. As for the negatively charged divacancy V_2^-, it is found that the RB

TABLE I. Total energy difference and rebond lengths, d_{12} and d_{23}, of divacancy V_2 in Si for negatively charged (−), neutral (0), and positively charged (+) states. Results from the supercell models with 64 sites, 216 sites, 512 sites, and 1000 sites are shown along with the results from the cluster model, $Si_{246}H_{186}$. The three relaxation patterns, i.e., the resonant bond (RB), the small pairing (SP), and the large pairing (LP), are examined. The total energy E is represented by its difference from that of the RB configuration E_{RB} for each charge state. In the cluster model, the results in Refs. 22 and 23 are also shown in parentheses.

Model		d_{12} (Å)	d_{23} (Å)	$E-E_{RB}$ (meV)
	RB(−)	3.59	3.48	0
	SP(−)	3.49	3.57	+0.4
64-site	RB(0)	3.68	3.46	0
supercell	SP(0)	3.46	3.57	+5.0
(LDA)				
	RB(+)	3.69	3.54	0
	SP(+)	3.56	3.66	+3.0
	RB(−)	3.39	3.15	0
	SP(−)	3.06	3.31	+2.0
216-site	RB(0)	3.50	2.95	0
supercell	SP(0)	2.80	3.37	+7.0
(LDA)				
	RB(+)	3.50	3.06	0
	SP(+)	2.89	3.42	+18.0
	RB(−)	3.35	3.11	0
	SP(−)	3.01	3.29	+6.00
	LP(−)	2.69	3.32	+13.7
512-site	RB(0)	3.48	2.86	0
supercell	SP(0)	2.77	3.33	+22.0
(LDA)	LP(0)	2.75	3.34	+19.0
	RB(+)	3.48	2.88	0
	SP(+)	2.80	3.37	+20.0
	LP(+)	2.75	3.34	+19.0
512-site	RB(−)	3.56	3.27	0
supercell	SP(−)	3.12	3.46	+6.00
(GGA)	LP(−)	2.79	3.47	+104.0
1000-site	RB(−)	3.36	3.09	0
supercell	SP(−)	2.96	3.26	+17.5
(LDA)	LP(−)	2.69	3.33	+23.7
	RB(−)	3.40	3.23	0
		(3.34)	(3.17)	(0)
$Si_{246}H_{186}$	SP(−)	3.11	3.35	−15.5
cluster				
(LDA)	LP(−)	2.77	3.35	+42.9
		(2.76)	(3.30)	(−120.0)

configuration is energetically most favorable. The SP configuration is also found to be stable. Yet, its formation energy is larger than that of the RB configuration by about 10 meV. We have also found that the LP configuration also exists when we use supercells in which more than 512 sites are included. Interestingly, the LP configuration does not appear with smaller supercells in accord with the previous supercell calculations.[17–19,40] This means that the large scale calculation is necessary not only for quantitative descriptions but also for qualitative descriptions of the Si divacancies. The formation energy of the LP configuration is, however, systematically larger than that of the RB configuration by 10–20 meV. It is found that the RB configuration is the lowest in energy, the SP is the next, and the LP is the highest when it exists, whatever the size of the supercell is.

Results of GGA calculations for negatively charged divacancies by using the 512-site supercells are also shown in Table I. In GGA, the lattice constant is slightly longer than that of LDA. We find that the rebond lengths also tend to be longer than those of LDA. Although the LP configuration is much higher in energy compared to that of LDA, the following conclusion is unchanged by our GGA calculations: The RB configuration is the lowest in energy, the SP is the next, and the LP configuration exists and is the highest in energy.

As for the neutral and positively charged V_2, we have found that the RB configuration is again energetically most favorable. The LP configuration does not appear with the supercells in which less than 216 sites are included, as it does not for V_2^-. The calculated total energies for the RB configuration is lower than the LP and the SP configurations by about 20 meV when we use 512-site supercell. The energetics among the RB, SP, and LP configurations for neutral and positively charged states obtained in the 512-site supercell is likely to hold for the 1000-site supercell since the convergence with respect to the cell size has been well established by calculations for the negatively charged state.

The calculated lengths of the rebonds converge with respect to the cell size in the present supercell calculations, as shown in Table I. Interestingly, the lengths of the rebonds show characteristic variation depending on the charge states and on the relaxation patterns (Table I). In the SP configuration, the length of the rebond d_{12} decreases from the positively charged state to the neutral state. Then, the length increases from the neutral to the negatively charged state. This is interpreted by the molecular orbital picture presented in Sec. II. In the positively charged and the neutral states, electrons are accommodated in b_u^2 state which has a bonding character between the two pairing atoms. Hence, the rebond length d_{12} becomes shorter upon accommodation of an additional electron in the neutral state. In the negatively charged state, another electron is accommodated in a_u state which has an antibonding character. Thus, the rebond length d_{12} becomes longer in the negatively charged state. Figure 5(a) shows the highest occupied state for the negatively charged SP configuration that indeed shows the antibonding character for the pairing.

In the RB and the LP configurations, the third electron in the negatively charged state is accommodated in the b_u and a_g^2 states, respectively. Both states have bonding characters between atoms 1 and 2. Thus, the rebond length d_{12} becomes short compared with the neutral or the positively charged state in the RB and the LP configurations. Figure 5(b) shows the bonding character of the highest occupied state in the negatively charged LP configuration.

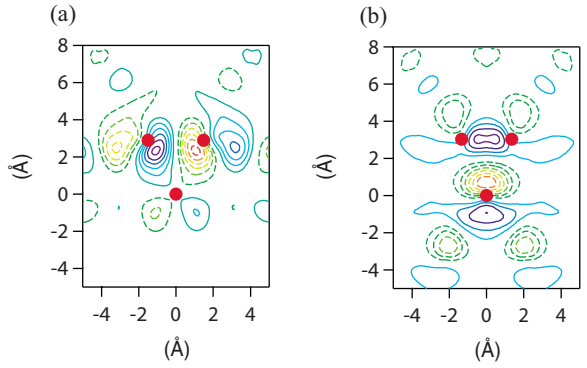

FIG. 5. (Color online) Highest occupied Kohn–Sham orbitals of V_2^- in (a) SP and (b) LP configurations. Contours are plotted on the (111) plane, which includes the atoms (1,2,3) [or (4,5,6)] shown in Fig. 1, with the equal difference of 0.01 bohr^{-3} between the contours. Solid and dashed lines depict the positive and negative values, respectively. Black balls show the positions of those atoms.

In the neutral and positively charged states, the structures and the energetics of the LP configurations are similar to those of SP configurations. In the neutral and positively charged states, the electrons are accommodated in the b_u states for both SP and LP configurations, so that the character of the electronic bonding is almost same. The only difference between the SP and LP is that the level alternation occur in the highest unoccupied electronic states a_u and a_g (see Fig. 2).

We have also performed the total-energy electronic-structure calculations for V_2^- using the cluster model. The cluster we have adopted is $Si_{246}H_{186}$ in which Si atoms within the 13th shell around the vacant sites and additional Si atoms up to the 25th shell along the ⟨110⟩ direction as well as H atoms attached to the outermost Si atoms are included. This cluster is as large as the cluster investigated in the past.[22,23] We have found that the three configurations, the RB, the LP, and the SP configurations, exist in this cluster model. In the previous cluster calculations in the real-space formulation using the same size of the cluster,[22,23] the SP configuration is not reported. The obtained rebond lengths in the present calculations shown in Table I are approximately the same with those in the previous calculations[22,23] within about 0.05 Å. This small difference may cause the total-energy difference of the order of 10 meV, judging from our careful examination using the supercell model.

We have found that the LP configuration is energetically unfavorable compared with the SP and the RB configurations. This is in accord with the supercell calculations described above. However, the most stable configuration is the SP configuration for this cluster and the RB configuration which is the ground state configuration in the supercell model is higher in energy by 15 meV. We have computed the root mean squares of atomic coordinates between the cluster model and the supercell model with 1000 atomic sites. The root mean square values are 0.03, 0.02, and 0.02 Å for the RB, the SP, and the LP configurations, respectively.

Hydrogen termination in the cluster model is suitable to remove redundant dangling bonds at the cluster boundary. It is an artifact, however, and may cause modulation of the charge density distribution. Comparing the calculated charge densities in the supercell model and in the cluster model, we find that electrons prefer to be distributed near hydrogen atoms and thus the distribution near the divacancy is also slightly different between the supercell and the cluster models. This may be a reason that the RB configuration is the most stable in the supercell model, whereas the SP configuration is in the cluster model.

TABLE II. Total energy differences (meV) among the RB, the SP and the LP configurations for V_2^- under uniaxial strains along [110] direction. The strains are given in Å. The energy is measured from that of the RB configuration. The supercell model with 512-site cell is used.

	Total energy (meV)		
Strain	Resonant bond	Small paring	Large paring
0.005	0	−13	−7
0.05	0	−140	−233

A systematic increase of supercell size in the present work strongly supports the RB configuration as a ground state. The 1000-site supercell contains all the Si atoms in the $Si_{246}H_{186}$ cluster. Hence, we provisionally conclude that the RB configuration is the ground state in LDA and in GGA in the density-functional theory.

In the ESR experiments,[12] the uniaxial stress is applied to obtain the direction of the displacement of the nearest neighbor Si atoms. Based on the data, the pairing-type configuration has been proposed. The applied stress in the experiment is along the ⟨110⟩ direction and the value is about 85 MPa. When we use Young's modulus of Si crystal [169.7 GPa (Ref. 41)], this stress corresponds to the strain of about 0.003 Å. This situation is different from the DFT calculations presented above.

We have therefore performed total-energy electronic-structure calculations for V_2^- with the RB, the SP, and the LP configurations under an uniaxial stress along the ⟨110⟩ direction. In the calculations, we introduce the strain δ along the [110] direction. Consequently, the expansion along the $[1\bar{1}0]$ direction takes place: i.e., the square (001) face of the original cubic supercell becomes rhombic. We have used the supercell model with 512 sites and examined two strains δ =0.005 Å and δ=0.05 Å. Table II shows the calculated total energies for the three configurations. Even for the small strain (0.005 Å), the paring-type configurations (both SP and LP) are lower in energy than the RB configuration. When the amount of the strain becomes larger (0.05 Å), the LP configuration becomes the most stable structure among the three. This finding that the pairing configurations become energetically favorable under the uniaxial stress is a key to reconcile the apparent discrepancy between the ESR experiment and the present DFT calculations. Even in the small strain of 0.005 Å, substantial portion of V_2^- is expected to be the LP configuration. We thus argue that the ground state configuration of V_2^- is the RB configuration and that the LP configuration becomes favorable under uniaxial stress and is de-

tected by EPR measurement. For the positively charged divacancy V_2^+, we expect that the same stress-induced paring configuration is responsible for the EPR signal.

V. SUMMARY

We have performed total-energy electronic-structure calculations with the LDA and the GGA in the density-functional theory for the divacancy in Si. A real-space finite-difference pseudopotential method has been developed in order to carry out large-scale calculations that provides unambiguous theoretical results which clarify the discrepancy among the calculations and the experiments in the past as to the structure of the Si divacancy. Supercell models containing up to 1000 sites as well as a cluster model containing 432 atoms are used to simulate the divacancy in an otherwise perfect crystal. The present LDA calculations with systematic increase of the supercell size indicate that the RB configuration is the most stable structure, the SP configuration is the next, and the LP configuration is the least stable for negatively and positively charged as well as neutral divacancies. The energy differences among the three configurations are found to be the order of 10 meV. The LDA calculations with the cluster model also show that the LP configuration is the least stable, although the SP configuration is the most stable in this case. Interesting variations of rebond lengths among different charge states have been found and interpreted in terms of the bonding and antibonding characters of the corresponding deep levels. We also perform GGA calculations with 512-site supercells and confirm that the overall conclusion obtained from the LDA calculations is unchanged by the GGA calculations, indicating that the RB configuration is the ground state of the Si divacancy in DFT using the supercell model. Yet the total-energy difference among the three configurations is an order of 10 meV in certain cases which is almost an extreme of the accuracy in the DFT calculations.

Considering situations of ESR measurements which determine the directions of the displacements of neighboring atoms, we have also performed the total-energy electronic-structure calculations under uniaxial stress along the $\langle 110 \rangle$ direction. We have found that induced strains alter the energetics and the SP and then the LP configurations become most stable with increasing strains. Based on this finding, we argue that the ground state configuration of the Si divacancy is the RB configuration and the pairing configurations become stable under the uniaxial stress and are detected by the EPR measurements.

ACKNOWLEDGMENTS

This work was partly supported by grants-in-aid from Ministry of Education, Culture, Sports, Science and Technology (MEXT), Japan under Contract No. 17064002. Computations were done at Science Information Processing Center, University of Tsukuba, at Institute for Solid State Physics, University of Tokyo, at Research Center of the Computational Science, Okazaki National Institute, and at Center for Computational Sciences (PACS-CS), University of Tsukuba.

[1] See, e.g., M. Lannoo and J. Bourgoin, *Point Defects in Semiconductors* (Springer, Berlin, 1983).
[2] For a review, S. T. Pantelides, Rev. Mod. Phys. **50**, 797 (1978).
[3] For a review, *Deep Centers in Semiconductors*, edited by S. T. Pantelides (Gordon and Breach, New York, 1986).
[4] G. D. Watkins and J. W. Corbett, Phys. Rev. **121**, 1001 (1961).
[5] J. W. Corbett, G. W. Watkins, R. M. Chrenko, and R. S. MacDonald, Phys. Rev. **121**, 1015 (1961).
[6] G. D. Watkins and J. W. Corbett, Phys. Rev. **134**, A1359 (1964).
[7] J. Bernholc, N. O. Lipari, and S. T. Pantelides, Phys. Rev. Lett. **41**, 895 (1978); Phys. Rev. B **21**, 3545 (1980).
[8] G. A. Baraff and M. Schlüter, Phys. Rev. Lett. **41**, 892 (1978); Phys. Rev. B **19**, 4965 (1979).
[9] G. A. Baraff, E. O. Kane, and M. Schlüter, Phys. Rev. Lett. **43**, 956 (1979).
[10] O. Sugino and A. Oshiyama, Phys. Rev. Lett. **68**, 1858 (1992).
[11] A. Antonelli, E. Kaxiras, and D. J. Chadi, Phys. Rev. Lett. **81**, 2088 (1998).
[12] G. D. Watkins and J. W. Corbett, Phys. Rev. **138**, A543 (1965).
[13] O. Sugino and A. Oshiyama, Phys. Rev. B **42**, 11869 (1990).
[14] C. A. J. Ammerlaan and G. D. Watkins, Phys. Rev. B **5**, 3988 (1972).
[15] J. G. de Wit, E. G. Sieverts, and C. A. J. Ammerlaan, Phys. Rev. B **14**, 3494 (1976).
[16] E. G. Sieverts, S. H. Muller, and C. A. J. Ammerlaan, Phys. Rev. B **18**, 6834 (1978).
[17] M. Saito and A. Oshiyama, Phys. Rev. Lett. **73**, 866 (1994).
[18] H. Seong and L. J. Lewis, Phys. Rev. B **53**, 9791 (1996).
[19] M. Pesola, J. von Boehm, S. Pöykkö, and R. M. Nieminen, Phys. Rev. B **58**, 1106 (1998).
[20] F. El-Mellouhi and N. Mousseau, Phys. Rev. B **71**, 125207 (2005).
[21] D. V. Makhov and L. J. Lewis, Phys. Rev. B **72**, 073306 (2005).
[22] S. Ögüt and J. R. Chelikowsky, Phys. Rev. Lett. **83**, 3852 (1999).
[23] S. Ögüt and J. R. Chelikowsky, Phys. Rev. B **64**, 245206 (2001).
[24] A methodology based on the scattering theory is free from ambiguity as to the boundary conditions of the electron states: J. Bernholc, N. O. Lipari, and S. T. Pantelides, Phys. Rev. Lett. **41**, 895 (1978); G. A. Baraff and M. Schlüter, *ibid.* **41**, 892 (1978). Determination of the scattering region and its effects on the energetics are still unresolved: R. Car, P. J. Kelly, A. Oshiyama, and S. T. Pantelides, Phys. Rev. Lett. **52**, 1814 (1984); **54**, 360 (1985).
[25] P. Hohenberg and W. Kohn, Phys. Rev. **136**, B864 (1964).
[26] W. Kohn and L. J. Sham, Phys. Rev. **140**, A1133 (1965).
[27] J. P. Perdew and A. Zunger, Phys. Rev. B **23**, 5048 (1981); D. M. Ceperley and B. J. Alder, Phys. Rev. Lett. **45**, 566 (1980).
[28] J. P. Perdew, K. Burke, and M. Ernzerhof, Phys. Rev. Lett. **77**, 3865 (1996).
[29] G. B. Bachelet, D. R. Hamann, and M. Schlüter, Phys. Rev. B **26**, 4199 (1982).
[30] N. Troullier and J. L. Martins, Phys. Rev. B **43**, 1993 (1991).

[31] J. R. Chelikowsky, N. Troullier, and Y. Saad, Phys. Rev. Lett. **72**, 1240 (1994); J. R. Chelikowsky, N. Troullier, K. Wu, and Y. Saad, Phys. Rev. B **50**, 11355 (1994).

[32] J.-I. Iwata, A. Oshiyama, and K. Shiraishi, Physica B **376-377**, 196 (2006).

[33] For the plane-wave basis-set calculations, we use Tokyo *ab initio* program package (TAPP) developed by a consortium initiated at University of Tokyo: J. Yamauchi, M. Tsukada, S. Watanabe, and O. Sugino, Phys. Rev. B **54**, 5586 (1996); H. Kageshima and K. Shiraishi, *ibid.* **56**, 14985 (1997); O. Sugino and A. Oshiyama, Phys. Rev. Lett. **68**, 1858 (1992).

[34] D. M. Bylander, L. Kleinman, and S. Lee, Phys. Rev. B **42**, 1394 (1990).

[35] G. Kresse and J. Furthmüller, Phys. Rev. B **54**, 11169 (1996).

[36] L. Kleinman and D. M. Bylander, Phys. Rev. Lett. **48**, 1425 (1982).

[37] L.-W. Wang, Phys. Rev. B **64**, 201107(R) (2001).

[38] L. C. Balbás, José Luís Martins, and José M. Soler, Phys. Rev. B **64**, 165110 (2001).

[39] J.-W. Jeong and A. Oshiyama, Phys. Rev. B **64**, 235204 (2001).

[40] In Ref. 21 Mahkov and Lewis call their paring-type structure the large paring. Judging from their level structures, however, it seems that their structure is the small-paring type.

[41] H. J. McSkimin, W. L. Bond, E. Buehler, and G. K. Teal, Phys. Rev. **83**, 1080 (1951).